


Biphase as a diagnostic for scale interactions in wall-bounded turbulenceG. Cui * and I. Jacobi*Faculty of Aerospace Engineering, Technion Israel Institute of Technology, Haifa 32000, Israel*

(Received 31 August 2020; accepted 12 January 2021; published 26 January 2021)

The phase of the bispectrum of a turbulent velocity signal is presented as a unified tool to relate the geometry and energetics of interactions between large- and small-scale motions in wall-bounded turbulence. The normalized bispectrum naturally describes nonlinear triadic interactions and thus is ideally suited for measuring the magnitude of coupling between the different scales of turbulence without the use of filtering procedures. In this study, the corresponding biphase is shown to represent the delay between large and small scales imposed by convective interactions and simultaneously to describe the direction of the turbulent streamwise energy cascade. The bispectrum and biphase are measured from a direct numerical simulation of a high-Reynolds-number channel flow and used to illustrate the relationship between the relative geometry of the interacting scales, the interaction delay, and the cascade of energy between them, offering an integrated perspective on scale interactions in turbulence through a single statistic.

DOI: [10.1103/PhysRevFluids.6.014604](https://doi.org/10.1103/PhysRevFluids.6.014604)**I. INTRODUCTION**

The interaction between large- and small-scale coherent structures in wall-bounded turbulence has been recognized since Rao *et al.* [1] reported that small-scale bursting events near the wall were characterized by the timescales of large-scale features in the outer flow. Bandyopadhyay and Hussain [2] introduced a systemic approach to studying these interscale interactions by calculating the cross correlation between a low-pass-filtered velocity signal (representing the large scales) and the rectified envelope of the remaining high-frequency signal content (the corresponding small scales). This cross-correlation approach was rediscovered and refined by the work of Mathis *et al.* [3], where the cross-correlation function was consolidated into a correlation coefficient \mathcal{R} that was interpreted to represent amplitude modulation by the large scales. Subsequent investigators applied these correlation coefficients to the transverse velocity components (e.g., [4]) and defined new correlation coefficients to distinguish amplitude from frequency modulation (e.g., [5]). Jacobi and McKeon [6] reconsidered the full cross-correlation function and analyzed its spectral analog, the cross spectrum, to study the modulation effect on a scale by scale basis, showing that very-large-scale motions (VLSMs) were the most significant contributor to the perceived modulation of the small scales.

The similarity between the cross-correlation coefficient for amplitude modulation and the skewness moment of the fluctuating velocity was recognized early on by Mathis *et al.* [3]. Schlatter and Örlü [7] showed that \mathcal{R} was indeed dependent on the skewness, and Mathis *et al.* [8] derived the precise form of this dependence via scale decomposition, indicating that the scale-decomposed skewness can provide an alternative perspective on the amplitude modulation process. Duvvuri and McKeon [9] performed a formal analysis of the correlation coefficient and skewness moment and showed that both represent a phase lag between triadically interacting velocity modes in the

*guangyao.cui@campus.technion.ac.il

turbulent boundary layer, consistent with the earlier phase interpretation of Chung and McKeon [10]. The fact that the amplitude modulation coefficient represents phase differences between wave-number triads is highly significant in light of the fact that the convective nonlinearity of the incompressible Navier-Stokes equations allows only nonlinear interactions between triadically coupled wave numbers \mathbf{k}' , \mathbf{k}'' , and $\mathbf{k} = \mathbf{k}' + \mathbf{k}''$. Therefore, the correlation coefficients between large- and small-scale motions reflect a fundamental feature of the convective nonlinearity in turbulent flows which may have important implications for modeling and prediction.

The consensus of previous investigations is that amplitude fluctuations in the small-scale turbulence occur downstream of corresponding fluctuations in the large scales, although the relationship between this phase lead of the small scales and the energy transfer between different scales has not been fully explored. However, the general question of the correspondence between specific coherent motions and the turbulent energy cascade has been studied extensively in the context of resolved and unresolved scales in large-eddy simulations. Piomelli *et al.* [11] observed that events of intense interscale energy transfer are found in close spatial proximity to strong sweeps. More recent computational experiments by Dong *et al.* [12] have identified specific spatial orientations between coherent sweeps, ejections, and regions of interscale energy transfer. Works by Cimarelli *et al.* [13,14] and Lee and Moser [15] have shown that spatially localized inverse energy cascades are a significant feature of wall-bounded flows, and Kawata and Alfredsson [16] demonstrated that the cascade of Reynolds stress fluctuations is inverse, opposite that of turbulent kinetic energy, thus indicating again the important connections between the local structural picture of turbulence and the energy transfer dynamics.

In this study, we apply a new tool to the scale-interaction problem in turbulence: the biphasic. We first show how the bispectrum and its corresponding biphasic are the natural diagnostics with which to explore the triadic interactions between large- and small-scales and that they can be utilized without any arbitrary signal filtering. Through a simple toy-problem, we show how the biphasic captures the essential phase information of the earlier cross-correlation analysis while also providing a simple energetic interpretation of the phase-relationship between scales. Finally, we report bispectrum and biphasic measurements from a high Reynolds number, turbulent channel flow and interpret them in the context of the physical orientation, interaction delays, and energy transfer between different streamwise scales of motion.

II. CORRELATION COEFFICIENTS, PHASE LAG, AND BIPHASE

A. Triadic interactions and quadratic phase coupling

We assume that a statistically stationary, streamwise fluctuating velocity signal $u(x)$ can be decomposed into its Fourier modes with wave numbers k_n , amplitudes α_n , and phases ϕ_{k_n} over a finite domain (epoch) of length L with M total spatial points, where the mean has been removed via a Reynolds decomposition over many epochs. All quantities are assumed to be nondimensional with respect to the channel half-height h and bulk velocity U :

$$u(x) = \sum_{n=1}^{M/2} \alpha_n \cos(k_n x + \phi_{k_n}), \quad k_n = \frac{2\pi n}{L}. \quad (1)$$

Out of all the modes in this signal, only triadically coupled modes contribute to the streamwise momentum and turbulent kinetic energy at a particular scale k and thus we consider just a single triad associated with that wave number $k' + k'' = k$ for $0 < k' < k'' < k$, with uniformly random phases $\phi_{k'}$, $\phi_{k''}$, and ϕ_k distributed between $[-\pi, \pi]$ such that

$$u(x) = \alpha_{k'} \cos(k'x + \phi_{k'}) + \alpha_{k''} \cos(k''x + \phi_{k''}) + \{\alpha_k \cos(kx + \phi_k) + \alpha_{k'} \cos(k'x + \phi_{k'}) \alpha_{k''} \cos(k''x + \phi_{k''})\}, \quad (2)$$

where we have explicitly included the possibility that the spectral power measured at wave number k may be the result of convective (quadratic) interactions between the other two wave numbers k' and k'' , which combine triadically to contribute at k , in a process known as quadratic phase coupling (QPC). Expanding the signal trigonometrically and labeling the mode amplitudes of the QPC and uncoupled terms as α_{QPC} and α_{uc} , respectively, we obtain

$$u(x) = \alpha_{k'} \cos(k'x + \phi_{k'}) + \alpha_{k''} \cos(k''x + \phi_{k''}) + \alpha_{\text{uc}} \cos(kx + \phi_{\text{uc}}) + \alpha_{\text{QPC}} \cos(kx + \phi_{k'} + \phi_{k''} + \Delta\phi_k), \quad (3)$$

where we have dropped the contribution at $(k' - k'')$ for simplicity, assuming all wave numbers in the triad are positive.

Finally, following Shils *et al.* [17] and Jamšek *et al.* [18], we have explicitly included in (3) the possibility that this quadratic interaction precedes a potentially wave-number-dependent phase delay $\Delta\phi_k$. The functional form of that phase delay $\Delta\phi_k$ determines its physical interpretation, as discussed by Preis [19] and briefly reviewed here. A wave-number-independent delay $\Delta\phi_k = \Delta\phi_0$ is referred to as an intercept delay. Every output k of the triadic interaction experiences an identical phase shift with respect to a pure triadic interaction without delay, and thus a signal constructed from all of the different triadic output wave numbers appears distorted. A sinusoidal signal experiencing an intercept delay will appear as the sum of two copies of itself: one phase shifted by $\pi/2$, with amplitude magnified by $\sin(\Delta\phi_0)$, and another in phase, with amplitude magnified by $\cos(\Delta\phi_0)$ [20]. Thus, triadic mode interactions with intercept delays can be observed via their effect on the amplitude of the resulting signals. A linear phase delay $\Delta\phi_k = k\Delta x$ means that the magnitude of the delay for each triad is proportional to its wave number k with a constant slope Δx . Because each triad is shifted in phase proportional to its wave number, the overall signal constructed from all of the different triadic outputs will appear undistorted but shifted in space by Δx . A linear phase delay is typically interpreted in nonlinear system analysis to reflect finite transport times for the interacting modes to arrive at or depart from the interaction site or (in a temporal sense) finite interaction times between those modes. Applying the spatial interpretation here, the presence of a linear phase delay would indicate that all of the small-scale modes k resulting from interacting large scales are shifted from the interaction site by a distance Δx such that for $\Delta x < 0$ the small scale appears farther downstream. Combinations of intercept and linear delays, written as $\Delta\phi_0 + k\Delta x$, are also possible, along with more complicated, nonlinear phase delays that describe significant phase distortion between different interacting triads.

B. Phase of the amplitude modulation coefficient

Applying the scale interaction analysis of [3], we low-pass filter the velocity signal at cutoff wave number k_c , where $k' < k_c < k'' < k$, to obtain the large-scale signal $u_L = \alpha_{k'} \cos(k'x + \phi_{k'})$. The small-scale signal is simply the remainder $u_S(x) = u - u_L$. The envelope of the small-scale signal $\mathcal{E}(x)$ is obtained from the magnitude of the analytic signal of u_S via its Hilbert transform $\mathcal{H}(x)$:

$$\begin{aligned} \mathcal{E} &= u_S^2(x) + \mathcal{H}(x)^2 \\ &= \alpha_{k'}^2 + \alpha_{\text{uc}}^2 + \alpha_{\text{QPC}}^2 + 2\alpha_{k''}\alpha_{\text{uc}} \cos(k'x - \phi_{k''} + \phi_{\text{uc}}) + 2\alpha_{k''}\alpha_{\text{QPC}} \cos(k'x + \phi_{k'} + \Delta\phi_k) \\ &\quad + 2\alpha_{\text{uc}}\alpha_{\text{QPC}} \cos(\phi_{\text{uc}} - \phi_{k'} - \phi_{k''} - \Delta\phi_k). \end{aligned}$$

Mathis *et al.* [3] calculated the correlation coefficient \mathcal{R} between u_L and the filtered envelope \mathcal{E} . However, Chung and McKeon [10] noted that this correlation coefficient can be interpreted as the cosine of the phase difference $\Delta\Phi_{k'}$ between the two signals at wave number k' such that $\mathcal{R} = \cos(\Delta\Phi_{k'})$. The sign of this phase difference is obscured by the cosine but can be revealed directly via the Fourier transform of the cross correlation

$$\Delta\Phi_{k'} = -\arg\{\hat{u}_L(k')\hat{\mathcal{E}}^*(k')\}, \quad (4)$$

where $\hat{(\cdot)}$ represents the finite Fourier transform, $\langle \cdot \rangle = \frac{1}{N} \sum_{n=1}^N (\cdot)$ represents the ensemble averaging over N epochs of measurements, where each epoch has random phases ($\phi_{k'}$, $\phi_{k''}$, and ϕ_{uc}), and the asterisk denotes the complex conjugate. The negative sign is due to complex conjugation in the cross-correlation theorem. Substituting the Fourier-transformed signals and expanding the ensemble averaging yields

$$\begin{aligned} \Delta \Phi_{k'} &= -\arg \left\{ \left[\frac{\alpha_{k'}}{2} e^{i\phi_{k'}} [\alpha_{k''} \alpha_{uc} e^{-i(-\phi_{k''} + \phi_{uc})} + \alpha_{k''} \alpha_{QPC} e^{-i(\phi_{k'} + \Delta \phi_k)}] \right] \right\} \\ &= -\tan^{-1} \left\{ \frac{\sin(-\Delta \phi_k) + \frac{\alpha_{uc}}{\alpha_{QPC}} \langle \sin(\phi_{k'} + \phi_{k''} - \phi_{uc}) \rangle}{\cos(-\Delta \phi_k) + \frac{\alpha_{uc}}{\alpha_{QPC}} \langle \cos(\phi_{k'} + \phi_{k''} - \phi_{uc}) \rangle} \right\} \approx \Delta \phi_k. \end{aligned}$$

The phase difference between the filtered and enveloped signals is the same as the phase delay assumed for the nonlinear interaction, in the limit of large ensembles. This is consistent with the report of Duvvuri and McKeon [9] that only triadically coupled scales contribute to the correlation coefficient and its associated phase. The filtering and enveloping approach tends to indiscriminately include a wide range of scales in its correlation analysis instead of focusing on only the triadically coupled scales that actually matter. We will apply a more narrowly tailored process for studying scale coupling that focuses on just the nonlinearly interacting wave-number triads themselves.

C. Bispectrum and biphas

The ideal tool for studying quadratic nonlinear interactions is the bispectrum $B(k', k'')$, which is the third-order spectrum of a signal $u(x)$, defined as

$$B(k', k'') = \langle \hat{u}(k') \hat{u}(k'') \hat{u}^*(k' + k'') \rangle \quad (5)$$

such that the statistical skewness $\langle u^3 \rangle$ is related to the bispectrum by $\langle u^3 \rangle = \sum_{k', k''} B(k', k'')$. Unlike the traditional second-order power spectrum $S(k) = \langle \hat{u}(k) \hat{u}^*(k) \rangle$, the complex bispectrum preserves phase information between triadically interacting modes. For a complete background on the bispectrum, see the classic works by Hinich and Clay [21], Kim and Powers [22], and Fackrell *et al.* [23]. The bispectrum is most well known in the analysis of ocean waves but also appears prominently in turbulence studies, to analyze isotropic turbulence [24,25], phase locking between modes in transitional boundary layers [26], and, most recently, perturbed turbulent boundary layers [27].

The bispectrum is typically normalized by the second-order power spectrum and referred to as the bicoherence $b(k', k'')$. Although a number of normalizations are discussed in the literature (see [28]), the most straightforward defines bicoherence as

$$b(k', k'') = \frac{|B(k', k'')|}{\sqrt{S(k')S(k'')S(k' + k'')}}. \quad (6)$$

For the triadic signal considered above, the squared bicoherence is

$$b^2(k', k'') = \frac{\alpha_{QPC}^2 + \alpha_{uc}^2 |e^{i(\phi_{k'} + \phi_{k''} - \phi_{uc})}|^2 + 2\alpha_{QPC}\alpha_{uc} \text{Re}\{e^{-i\Delta \phi_k} (e^{i(\phi_{k'} + \phi_{k''} - \phi_{uc})})\}}{\alpha_{QPC}^2 + \alpha_{uc}^2 + 2\alpha_{QPC}\alpha_{uc} \langle \cos(\phi_{k'} + \phi_{k''} - \phi_{uc} + \Delta \phi_k) \rangle}, \quad (7)$$

which, after ensemble averaging over the random phases, simplifies to $b^2 \approx \frac{\alpha_{QPC}^2}{\alpha_{QPC}^2 + \alpha_{uc}^2}$. Thus, the bicoherence represents the fraction of energy at wave number k associated with QPC from wave numbers k' and k'' . Greb and Rusbridge [29] note that for a signal with a continuous spectrum, the bicoherence will always be significantly smaller than unity, since many uncoupled triads will appear at the same wave number k where the coupling occurs. In other words, the α_{uc} factor will represent contributions from many different triads and can be approximated as $\alpha_{uc}^2 \sim M\alpha_{QPC}^2$, where M is the number of samples measured per epoch (which scales asymptotically with the number of triads).

TABLE I. Equivalent, spatial, phase delay measures and their physical significance in three different domains. For temporal phase measurements, like the hot-wire measurements, all of the signs should be reversed.

Domain	Phase measure	$(0, +\pi)$	$(-\pi, 0)$
correlation analysis	$-\Delta\Phi_{k'}, -k\Delta x, -\Delta\phi_k$	small scales lead	large scales lead
Fourier analysis	$\arg\{\hat{u}_L \hat{\mathcal{E}}^*\}$	small scales lead	large scales lead
bispectral analysis	$\beta(k', k'')$	forward cascade	reverse cascade

Therefore, bicoherences that are calculated using different epoch lengths M can be scaled by \sqrt{M} to validate convergence, as discussed in the Appendix.

As noted above, the detection of a phase lag in the correlation analysis is possible only in the presence of QPC, and the bicoherence indicates the magnitude of this QPC on a wave-number-by-wave-number basis, without the need for any filtering procedures. In other words, the presence of strong bicoherence identifies those velocity modes that most strongly contribute towards the phase lag. However, because the underlying bispectrum is complex, it also preserves the phase lag itself. The argument of the bispectrum is called the biphas $\beta(k', k'')$. Unlike the bispectrum, the biphas has not been widely utilized analytically [30]. For the triadic velocity signal above, the biphas is

$$\begin{aligned} \beta(k', k'') &= \arg\{\langle \alpha_{k'} \alpha_{k''} e^{i(\phi_{k'} + \phi_{k''})} (\alpha_{uc} e^{-i\phi_{uc}} + \alpha_{QPC} e^{-i(\phi_{k'} + \phi_{k''} + \Delta\phi_k)}) \rangle\} \\ &= \tan^{-1} \left\{ \frac{\sin(-\Delta\phi_k) + \frac{\alpha_{uc}}{\alpha_{QPC}} \langle \sin(\phi_{k'} + \phi_{k''} - \phi_{uc}) \rangle}{\cos(-\Delta\phi_k) + \frac{\alpha_{uc}}{\alpha_{QPC}} \langle \cos(\phi_{k'} + \phi_{k''} - \phi_{uc}) \rangle} \right\} \approx -\Delta\phi_k, \end{aligned}$$

which, in the ensemble limit, is precisely the Fourier phase difference measured between the large- and small-scale signals (and the negative of correlation phase $\Delta\Phi_{k'}$). Therefore, the phase difference obtained by the correlation analysis of the filtered signals corresponds to the negative biphas associated with any two large scales in a triadic phase-coupled interaction, obtained without any filtering. The equivalence of the different measures of phase lag, across the spatial, spectral, and bispectral domains, is summarized in Table I, where a linear phase delay $-k\Delta x$ is assumed for illustration only.

D. Biphas and energy cascade

The bispectrum and biphas are also intimately connected to the energy transfer between the different scales of a velocity mode triad. For homogeneous turbulence in the absence of mean gradients, the interscale energy transfer rate $\hat{T}(\mathbf{k})$ excluding the pressure transport contribution, for the turbulent kinetic energy density $\hat{E}(\mathbf{k}) = \langle \hat{u}_j(\mathbf{k}) \hat{u}_j^*(\mathbf{k}) \rangle$, is given by (see [31])

$$\hat{T}(\mathbf{k}) = k_n \delta_{jm} \text{Re} \left\{ i \sum_{k'} \langle \hat{u}_j(\mathbf{k}) \hat{u}_m^*(\mathbf{k}') \hat{u}_n^*(\mathbf{k} - \mathbf{k}') \rangle \right\}. \quad (8)$$

Considering just the energy transfer between streamwise modes at streamwise wave numbers $j = m = n = 1$ and $\mathbf{k} = (k, 0, 0)$, the transfer term can be simplified (using the natural symmetries of the bispectrum) as

$$\hat{T}(k) = -k \text{Im} \left\{ \sum_{k'} \langle \hat{u}(k) \hat{u}^*(k') \hat{u}^*(k - k') \rangle \right\} \quad (9)$$

$$= k \text{Im} \left\{ \sum_{k'+k''=k} B(k', k'') + \sum_{k'-k''=k} B(k', -k'') + \sum_{k''-k'=k} B(k'', k') \right\} \quad (10)$$

for $k', k'' > 0$. The interscale transfer includes three contributions from the bispectrum, reflecting different relative scales of velocity modes. The first term in (10) corresponds to the energy transfer from two larger scales k' and k'' to a smaller scale k , as we assumed above that $0 < k' < k'' < k$. The second and third terms represent energy transfer between combinations of mixed large and small scales. These three paradigms of energy transfer and their connection to the bispectrum were first identified by Yeh and Atta [32] and Wilson [33] and subsequently used extensively in atmospheric and stratified turbulence measurements [34,35]. The direction and magnitude of the streamwise energy cascade at scale k is therefore given by the sum of the triadic contributions defined through the bispectrum.

Focusing on just the transfer between large and small scales in the first term, the partial interscale flux $\Delta\hat{T}$ can be written as a sum of the imaginary parts of individual triadic transfers or, equivalently, the imaginary part of the cumulative transfer summed over all triads

$$\Delta\hat{T}(k) = k \sum_{k'+k''=k} |B(k', k'')| \sin[\beta(k', k'')] = kB_s(k) \sin[\beta_s(k)], \quad (11)$$

where the cumulative magnitude and corresponding average phase are denoted by B_s and β_s , respectively.

The individual triads within the summation represent the contribution to the energy cascade at k from the discrete larger modes k' and k'' . For $0 < \beta(k', k'') < \pi$, the transfer represents the classical (streamwise) energy cascade, with energy flowing towards the smaller scales. For $-\pi < \beta(k', k'') < 0$, the transfer represents a reverse cascade. Holding the bispectrum magnitude fixed, the optimal forward energy transfer occurs when $\beta(k', k'') = +\pi/2$, corresponding to the location of $\mathcal{R} = 0$ in the amplitude modulation framework and thus roughly corresponding to the outer spectral energy peak and the midpoint of the logarithmic region, as noted by Mathis *et al.* [3].

The biphasic shows that the phase lag $\Delta\Phi_{k'}$ (previously detected by filtering and correlation techniques) indicates not only a phase delay of the nonlinearly interacting modes, but also the direction of the energy transfer. Were there no delay between the interacting modes (i.e., $\beta = 0$) the streamwise energy transfer between large and small scales would be zero. A positive lag ($\beta > 0$) therefore indicates the presence of the classical forward energy cascade and a negative lag indicates an inverse cascade. The cumulative biphasic β_s represents the same orientation and energy transfer information, but in an averaged sense, over all triads summing to k . The biphasic and bispectrum combine energetic and spatial perspectives on the scale interaction problem.

III. BIPHASE BEHAVIOR IN THE TURBULENT CHANNEL

A. Channel computations

We present the bicoherence and biphasic calculations for a direct numerical simulation (DNS) of turbulent channel flow at $\text{Re}_\tau \approx 5200$ and interpret the biphasic with respect to the physical and energetic orientation of the different scales. The details of the DNS were reported by Lee and Moser [36]. Streamwise-wall-normal slices of the channel were $8\pi h \times 2h$ in extent, containing 10240×1536 physical nodes, with uniform streamwise resolution $\Delta x^+ = 12.7$. The slices were sampled from the full simulation at 11 different time instants (each separated by 0.7 flowthrough times) and at spanwise locations separated by $\Delta z^+ = 47.86$. Each slice was divided into four epochs: mirrored along the central y axis and divided in half in the streamwise direction, with $M_0 = 5120$ points per epoch. The epochs were averaged over their four-nearest neighbors in y , giving an effective y resolution that ranged from $\Delta y^+ = 0.67$ at the wall to $\Delta y^+ = 31.13$ at the channel center. The epochs were zero padded to twice their length and a Hanning window was applied prior to Fourier transformation with 50% overlap and the construction of the energy spectrum and bispectrum. The spectra were calculated from 1.5×10^5 total epochs and convergence was verified by varying the number and length of epochs, as discussed in the Appendix. Finally, the bicoherence was calculated

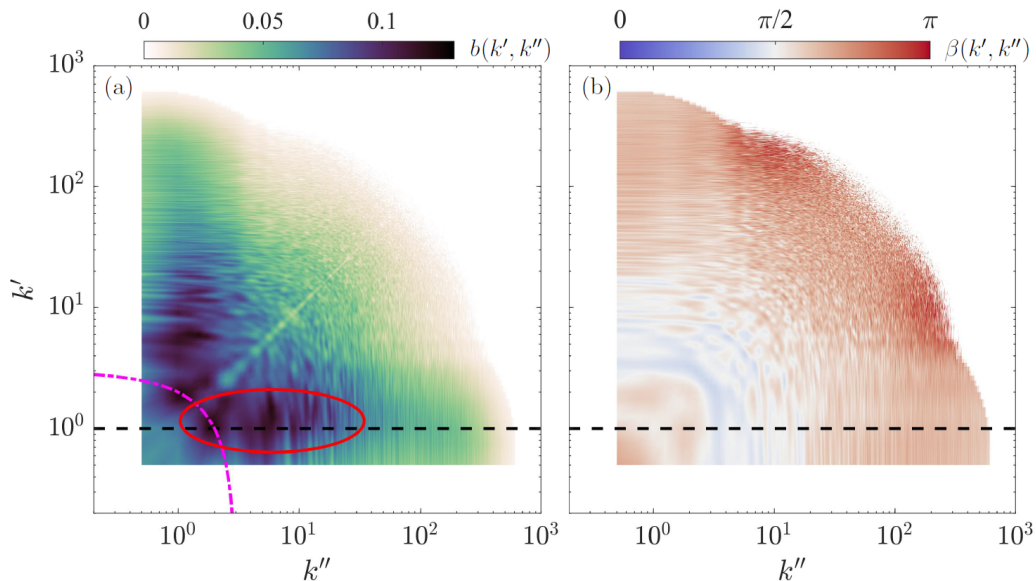


FIG. 1. (a) Bicoherence and (b) biphase maps near the outer spectral energy peak $y \approx 0.05$. The biphase has been thresholded to remove statistically insignificant phases. The horizontal dashed line marks the location for the bispectral slices shown in Fig. 2 and the red ellipse marks the region of intense bicoherence for scales coupled with the VLSMs. The magenta dash-dotted line indicates the line of constant $k = 3$ for the LSM associated with the highly coherent coupling.

by normalizing the bispectrum according to (6), taking care to avoid artifacts from the normalization by adding a small offset $\epsilon \approx 10^{-9}$, following the approach of Collis *et al.* [37].

B. Results: Phase delay measures

The bicoherence and biphase at $y \approx 0.05$ (with outer nondimensionalization, as above, corresponding to the location of the outer spectral energy peak) are shown in Fig. 1. At this location, the maximum bicoherence occurs around $(k', k'') \approx (1.5, 1.5)$, denoting nonlinear interactions between two VLSMs to produce another large-scale motion (LSM). However, relatively high bicoherence is observed along the whole line $k' = 1$ for all k'' (circled in red), thus indicating that the VLSM interacts nonlinearly with a wide range of smaller-scale motions.

In order to interpret the biphase map, values of the biphase that correspond to statistically insignificant levels of bicoherence are not physically meaningful and are thus eliminated [38] by constructing a 99% confidence interval about the squared bicoherence value $b^2 = 0$, utilizing the empirical observation [39] that the squared bicoherence multiplied by the ensemble size follows a χ^2 distribution with two degrees of freedom. The remaining physically meaningful biphase values are approximately circular Gaussian distributed across ensembles [40] with variance $\sigma_\beta^2 = \frac{1}{2N}(\frac{1}{b^2} - 1)$ and thus are expected to be statistically significant for large ensemble size N . After eliminating the nonmeaningful values of the biphase, it appears that the biphase everywhere in the bispectral plane is positive, indicating that the nonlinear interaction induces a phase delay consistent with the small-scale envelope leading the large scales, and a classical forward energy cascade from large to small scales.

The two-dimensional form of the bicoherence makes observing trends with respect to the wall-normal location difficult. Jeffries *et al.* [41] introduced the idea of slicing the bicoherence along lines of constant wave number k' and thus observing the variation with respect to k'' only. The variation of the bicoherence along the VLSM slice $k' = 1$ as a function y is shown in Fig. 2(a). The

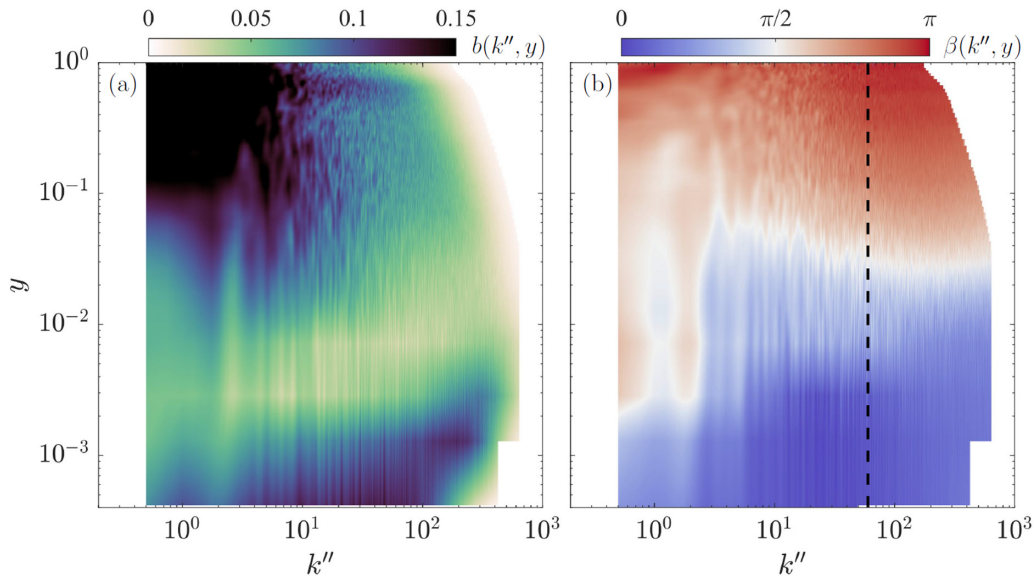


FIG. 2. (a) Sliced bicoherence and (b) sliced biphas along the VLSM slice $k' = 1$, corresponding to the dashed line in Fig. 1. These maps represent the nonlinear coupling and delay interactions between the VLSM scale and smaller scales within the flow.

sliced bicoherence indicates strong nonlinear coupling very near the wall and also near the channel centerline, between the VLSM and a broad range of smaller wave numbers, along with a region of milder coupling spread throughout the channel.

The sliced biphas in Fig. 2(b) is positive throughout the channel and at all wave numbers k'' coupled with $k' = 1$, varying from 0 near the wall to $+\pi$ near the centerline. The profile of the biphas appears remarkably uniform across the channel for all wave numbers $k'' \gtrsim 60$ (marked by the vertical dashed line), whereas for $k'' \lesssim 60$, the profile of the biphas is nonuniform over wave number. As noted above, the biphas captures the delay associated with the triadic interaction and the physical interpretation of that delay depends on the functional form of $\beta(k', k'')$. In this sliced biphas map, we observe both general types of interactions delays over different ranges of wave numbers. In the region of high wave numbers, where β is roughly constant with respect to k'' (and thus k also, since k' is held constant), the biphas indicates an intercept delay in the nonlinear interaction. Therefore, all of the small scales resulting from the VLSM interaction are shifted by a constant phase, resulting in a distortion of the small-scale signal in comparison to a pure triadic interaction. This distorted small-scale signal cannot be meaningfully interpreted as a spatial shift, since each wave number is shifted with respect to all others nonuniformly in space. By contrast, in the low-wave-number region, β varies with k'' according to the y location: Near the wall, β decreases with k'' and far from the wall, β increases with k'' . If the variation of β were perfectly linear with k (where $k = k' + k''$), then all of the different small scales resulting from the VLSM interactions would appear uniformly shifted in space with respect to the products of pure triadic interactions, without any distortion to the small-scale signal at all. Because the biphas variation is not perfectly linear, it represents some combination of uniform spatial delay across different triads and distortion between the different triads. In addition, because the slope of β with respect to k varies with wall-normal location, the implied spatial delay also depends on the wall-normal location, with $\Delta x > 0$ near the wall and the opposite far from the wall.

Aside from the delay information contained within the map of the biphas, individual biphas profiles can be used to highlight the energetic interpretation of the biphas. The biphas profiles for a single representative triad $(k', k'', k) = (1, 2, 3)$ and the average biphas profile $\beta_s(k = 3)$

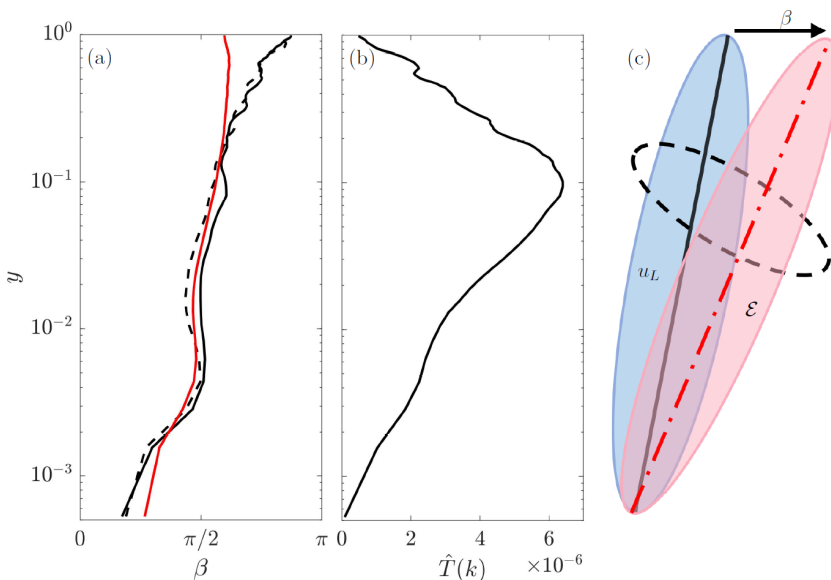


FIG. 3. (a) Biphase profile β for $(k', k'') = (1, 2)$ (black solid line), the average biphase profile β_s for all triads associated with $k = 3$ (black dashed line), and the phase $-\Delta\Phi_{k'}$ from the filtered cross-correlation approach (red solid line). (b) Profile of $\hat{T}(k)$ for $k = 3$, indicating the region of maximal, streamwise, interscale energy transfer just above the region where $\beta_s \approx +\pi/2$. (c) Relative orientation of u_L and \mathcal{E} for the forward streamwise energy cascade, illustrating the physical implication of the biphase. The dashed ellipse indicates the region of intense, interscale energy transfer.

associated with the interscale flux of all wave numbers (k', k'') triadically coupled to the same k are both shown in Fig. 3(a). The phase lag calculated via filtering from the amplitude modulation coefficient \mathcal{R} is also shown and the expected similarity is observed.

The biphase captures the nonlinear interaction delay between large and small scales on a wave-number-by-wave-number basis that had previously been available only via filtering on an average basis. Moreover, the biphase indicates that the phase lead of small scales is consistent with a forward cascade of streamwise interscale energy, thus connecting the (streamwise) energy cascade and scale orientation information in a single statistic. The physical interpretation of the biphase profile is illustrated in Fig. 3(c), where the region of intense streamwise energy transfer (circled in dashes) corresponds to the profile of $\hat{T}(k)$ in Fig. 3(b). The maximal interscale transport occurs in approximately the same neighborhood as the the region of $\beta \approx +\pi/2$, consistent with Eq. (11).

IV. CONCLUSION

The biphase was shown to naturally represent the phase lag between large- and small-scale motions in wall-bounded turbulence, without the use of filtering or enveloping procedures. Moreover, the normalized bispectrum allows for a measure of the magnitude of nonlinear phase coupling between scales, on a spectral basis, and can simultaneously be interpreted as an indication of the streamwise energy cascade between scales. Measurements of the biphase for a high-Reynolds-number turbulent channel flow were consistent with previous reports using cross correlations and conditional averaging techniques, confirming that the envelope of small-scale motions leads large scales in phase. However, the biphase also indicated that this phase lead was associated with the classical forward cascade of energy. Moreover, the biphase revealed that the phase lead represented a nonlinear interaction delay, which was shown to vary in functional form across different wave-number triads and different wall-normal locations, with each functional form leading to different

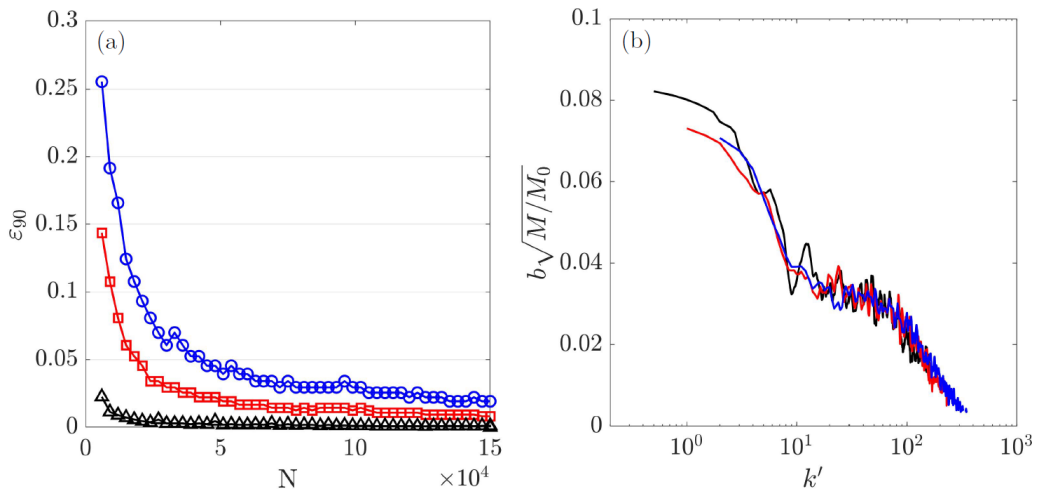


FIG. 4. (a) Upper bound of the relative error between different ensemble sizes for 90% of the wave numbers for the premultiplied energy spectral density (black triangles), the bicoherence (blue circles), and the biphase (red squares), measured at $y = 0.05$. (b) Collapse of diagonal slices of the bicoherence at $y = 0.05$ with different truncated epoch lengths M , normalized by the square root of their epoch length, compared to the full epoch length $M_0 = 5120$: $M = M_0$ (black line), $M = 0.5M_0$ (red line), and $M = 0.25M_0$ (blue line).

physical interpretations. The biphase represents an important tool in the ongoing effort to relate the structure and energetics of wall-bounded turbulence.

ACKNOWLEDGMENTS

This research was supported by Grant No. 1704/17 from the Israel Science Foundation. The authors thank an anonymous referee for helpful suggestions, particularly with respect to the spectral convergence.

The authors report no conflict of interest.

APPENDIX: BICOHERENCE AND BIPHASE CONVERGENCE

To examine the convergence of the bicoherence quantitatively, we define the relative error $\varepsilon(k', k''; N + \Delta N)$ between the bicoherence $b_{N+\Delta N}$ calculated from an ensemble of $N + \Delta N$ epochs with respect to the bicoherence b_N calculated from N epochs on a wave-number basis, according to

$$\varepsilon(k', k''; N) = |b_{N+\Delta N} - b_N| / |b_N|. \quad (\text{A1})$$

Then, for each ensemble N , we examine the cumulative density function of the resulting relative errors for all wave numbers and select the upper bound relative error ε_{90} that bounds 90% of the statistically significant bicoherence values. This upper bound represents the maximum relative variation in bicoherence level between different size ensembles. The same process was applied to the biphase and an analogous calculation was applied to the streamwise spectral energy density, for comparison, all shown in Fig. 4(a). As expected, the higher-order spectra converge more slowly than the spectral energy density and thus even with $N = 1.5 \times 10^5$ epochs (with $\Delta N = 3 \times 10^3$), the upper bound relative error appears larger, just below 2.0%, compared to the spectral energy density which is easily bounded by 0.1%. However, the use of relative error is also expected to behave differently in the two types of spectra, because the bicoherence values tend to be very small, which is known to artificially inflate relative errors via the denominator of (A1) [42]. The larger-magnitude biphase is bounded by 0.8%. Therefore, despite the slightly higher error bound, the very shallow

slope of ε_{90} with respect to N indicates that the spectra are adequately converged and no qualitative differences were observed among bicoherence maps even at significantly larger quantitative error bounds. The converged bicoherence values also depend on the epoch length used, as noted above. This epoch length dependence can be eliminated by normalization by the square root of the epoch length itself, as shown in Fig. 4(b).

-
- [1] K. N. Rao, R. Narasimha, and M. A. Narayanan, The ‘bursting’ phenomenon in a turbulent boundary layer, *J. Fluid Mech.* **48**, 339 (1971).
 - [2] P. R. Bandyopadhyay and A. K. M. F. Hussain, The coupling between scales in shear flows, *Phys. Fluids* **27**, 2221 (1984).
 - [3] R. Mathis, N. Hutchins, and I. Marusic, Large-scale amplitude modulation of the small-scale structures in turbulent boundary layers, *J. Fluid Mech.* **628**, 311 (2009).
 - [4] K. M. Talluru, R. Baidya, N. Hutchins, and I. Marusic, Amplitude modulation of all three velocity components in turbulent boundary layers, *J. Fluid Mech.* **746**, R1 (2014).
 - [5] W. J. Baars, K. M. Talluru, N. Hutchins, and I. Marusic, Wavelet analysis of wall turbulence to study large-scale modulation of small scales, *Exp. Fluids* **56**, 1 (2015).
 - [6] I. Jacobi and B. J. McKeon, Phase relationships between large and small scales in the turbulent boundary layer, *Exp. Fluids* **54**, 1481 (2013).
 - [7] P. Schlatter and R. Örlü, Quantifying the interaction between large and small scales in wall-bounded turbulent flows: A note of caution, *Phys. Fluids* **22**, 051704 (2010).
 - [8] R. Mathis, I. Marusic, N. Hutchins, and K. R. Sreenivasan, The relationship between the velocity skewness and the amplitude modulation of the small scale by the large scale in turbulent boundary layers, *Phys. Fluids* **23**, 121702 (2011).
 - [9] S. Duvvuri and B. J. McKeon, Triadic scale interactions in a turbulent boundary layer, *J. Fluid Mech.* **767**, R4 (2015).
 - [10] D. Chung and B. J. McKeon, Large-eddy simulation of large-scale structures in long channel flow, *J. Fluid Mech.* **661**, 341 (2010).
 - [11] U. Piomelli, Y. Yu, and R. J. Adrian, Subgrid-scale energy transfer and near-wall turbulence structure, *Phys. Fluids* **8**, 215 (1996).
 - [12] S. Dong, Y. Huang, X. Yuan, and A. Lozano-Durán, The coherent structure of the kinetic energy transfer in shear turbulence, *J. Fluid Mech.* **892**, A22 (2020).
 - [13] A. Cimarelli, E. De Angelis, and C. Casciola, Paths of energy in turbulent channel flows, *J. Fluid Mech.* **715**, 436 (2013).
 - [14] A. Cimarelli, E. De Angelis, J. Jimenez, and C. M. Casciola, Cascades and wall-normal fluxes in turbulent channel flows, *J. Fluid Mech.* **796**, 417 (2016).
 - [15] M. Lee and R. D. Moser, Spectral analysis of the budget equation in turbulent channel flows at high Reynolds number, *J. Fluid Mech.* **860**, 886 (2019).
 - [16] T. Kawata and P. H. Alfredsson, Inverse Interscale Transport of the Reynolds Shear Stress in Plane Couette Turbulence, *Phys. Rev. Lett.* **120**, 244501 (2018).
 - [17] J. Shils, M. Litt, B. Skolnick, M. Sperling, and M. Stecker, in *Proceedings of the 18th Annual International Conference of the IEEE Engineering in Medicine and Biology Society, Amsterdam, 1996*, edited by H. Boom, C. Robinson, W. Rutten, M. Neuman, and H. Wijkstra (IEEE, Amsterdam, 1996), p. 974.
 - [18] J. Jamšek, A. Stefanovska, P. V. E. McClintock, and I. A. Khovanov, Time-phase bispectral analysis, *Phys. Rev. E* **68**, 016201 (2003).
 - [19] D. Preis, Linear distortion, *J. Audio Eng. Soc.* **24**, 346 (1976).
 - [20] J. C. Steinberg, Effects of phase distortion on telephone quality, *Bell Syst. Tech. J.* **9**, 550 (1930).
 - [21] M. J. Hinich and C. S. Clay, The application of the discrete Fourier transform in the estimation of power spectra, coherence, and bispectra of geophysical data, *Rev. Geophys.* **6**, 347 (1968).

- [22] Y. C. Kim and E. J. Powers, Digital bispectral analysis and its applications to nonlinear wave interactions, *IEEE Trans. Plasma Sci.* **7**, 120 (1979).
- [23] J. W. Fackrell, P. R. White, J. K. Hammond, R. J. Pinnington, and A. T. Parsons, The interpretation of the bispectra of vibration signals—: II. Experimental results and applications, *Mech. Syst. Sign. Process.* **9**, 267 (1995).
- [24] C. W. Van Atta, Inertial range bispectra in turbulence, *Phys. Fluids* **22**, 1440 (1979).
- [25] J. R. Herring, Theoretical calculations of turbulent bispectra, *J. Fluid Mech.* **97**, 193 (1980).
- [26] T. Corke and R. Mangano, Resonant growth of three-dimensional modes in transitioning Blasius boundary layers, *J. Fluid Mech.* **209**, 93 (1989).
- [27] S. Midya, F. O. Thomas, and T. C. Corke, *Proceedings of the Tenth International Symposium on Turbulence and Shear Flow Phenomena, Chicago, 2017*, Session 7B-6, pp. 1–6.
- [28] M. J. Hinich and M. Wolinsky, Normalizing bispectra, *J. Stat. Plan. Infer.* **130**, 405 (2005).
- [29] U. Greb and M. G. Rusbridge, The interpretation of the bispectrum and bicoherence for non-linear interactions of continuous spectra, *Plasma Phys. Contr. Fusion* **30**, 537 (1988).
- [30] T. J. Maccarone, The biphase explained: Understanding the asymmetries in coupled Fourier components of astronomical time series, *Mon. Not. R. Astron. Soc.* **435**, 3547 (2013).
- [31] S. B. Pope, *Turbulent Flows* (Cambridge University Press, Cambridge, 2000).
- [32] T. Yeh and C. Atta, Spectral transfer of scalar and velocity fields in heated-grid turbulence, *J. Fluid Mech.* **58**, 233 (1973).
- [33] J. R. Wilson, Some observed statistical properties of small scale turbulence, Ph.D. thesis, University of British Columbia, Vancouver, Canada, 1974.
- [34] K. S. Lii, M. Rosenblatt, and C. W. Van Atta, Bispectral measurements in turbulence, *J. Fluid Mech.* **77**, 45 (1976).
- [35] K. N. Helland, E. C. Itsweire, and K. S. Li, A program for the computation of bispectra with application to spectral energy transfer in fluid turbulence, *Adv. Eng. Softw.* **7**, 22 (1985).
- [36] M. Lee and R. D. Moser, Direct numerical simulation of turbulent channel flow up to $Re_\tau \approx 5200$, *J. Fluid Mech.* **774**, 395 (2015).
- [37] W. B. Collis, P. R. White, and J. K. Hammond, Higher-order spectra: The bispectrum and trispectrum, *Mech. Syst. Sign. Process.* **12**, 375 (1998).
- [38] J. L. Shils, The bispectrum of the human electroencephalogram, Ph.D. thesis, University of Pennsylvania, 1995.
- [39] R. A. Haubrich, Earth noise, 5 to 500 millicycles per second: 1. Spectral stationarity, normality, and nonlinearity, *J. Geophys. Res.* **70**, 1415 (1965).
- [40] S. Elgar and G. Sebert, Statistics of bicoherence and biphase, *J. Geophys. Res.* **94**, 223 (1989).
- [41] W. Q. Jeffries, J. A. Chambers, and D. G. Infield, Experience with bicoherence of electrical power for condition monitoring of wind turbine blades, *IEEE Proc.: Vis. Image Sign. Process.* **145**, 141 (1998).
- [42] P. J. Roache, Perspective: A method for uniform reporting of grid refinement studies, *J. Fluid. Eng.* **116**, 405 (1994).